Catalysis Science & Technology

Accepted Manuscript

ROYAL SOCIETY OF CHEMISTRY

www.rsc.org/catalysis

Promoting effect of Nd on the reduction of NO with NH_3 over CeO_2 supported by activated semi-coke: an in situ DRIFTS study

*Yan Chen[a], Jinping Wang[a], Zheng Yan[b], Lili Liu[a], Zuotai Zhang[a], Xidong Wang[a]**

[a] *Beijing Key Laboratory for Solid Waste Utilization and Management, College of Engineering Peking University, Beijing 100871, China*

[b] *Liaoning Key Laboratory of Clean Energy and Institute of Clean Energy and Environmental Engineering, College of Energy and Environment Shenyang Aerospace University, Liaoning 110034, China*

*Corresponding Author's E-mail: xidong@pku.edu.cn

ABSTRACT

Cerium oxides and neodymium-cerium composite oxides were loaded onto the activated semi-coke (ASC) by hydrothermal method for the selective catalytic reduction (SCR) of NO with NH_3. The catalytic activity of CeO_2/ASC was greatly enhanced by the addition of Nd. The mechanistic cause of the promoting effect of Nd was systematically investigated using various characterizations, including XRD, SEM, TEM and in situ DRIFTS. The results revealed that the reaction route for NH_3-SCR followed both the E-R and L-H mechanisms over CeO_2/ASC and CeO_2-Nd/ASC catalysts. Nevertheless, Nd doping process was beneficial for the formation of Ce^{3+} and gave rise to the transformation of Lewis acid sites to Brønsted acid sites, which influenced the mechanism of SCR reaction. The generation of oxygen vacancies was in favor of the oxidation of NO to NO_2 and thereby facilitated the proceeding of the following reduction reactions. Thus, the presence of Ce^{3+} state and oxygen vacancies played the primary role for the improved low-temperature SCR performance of CeO_2-Nd/ASC catalyst.

1. Introduction

Nitrogen oxides (NO_x) in the flue gas are major air pollutants, which have caused serious environmental problems such as acid rain, photochemical smog, ozone depletion, low visibility and fine particulates.[1] Selective catalytic reduction (SCR) of NO_x with NH_3 has been proved to be one of the most efficient methods for the removal of NO_x and the widely used catalyst in commercial SCR system is the toxic V_2O_5-$WO_3(MoO_3)/TiO_2$ catalyst, which is only efficient within the narrow temperature window of 300-400 °C.[1,2] However, the presence of the fly ash and SO_2 in the flue gas inevitably results into the deactivation of catalyst due to pore plugging, coverage of active components and erosion[3-7] apart from the costly retrofit for the existing boiler system.[8,9] Hence, new environmentally friendly catalysts, which can exhibit high efficiencies (< 300 °C) at the downstream of the electrostatic precipitator and the desulfurization units, are of urgent need.

In recent years, novel catalysts based on cerium, manganese, iron and other transition metals have been extensively investigated.[10-19] Cerium-based catalysts have attracted increasing attention for their outstanding denitration performances due to their high oxygen storage capacity and excellent redox properties.[20-37] Moreover, better resistance for SO_2, H_2O and alkaline metals were achieved over this type of catalysts. In our previous work,[35] CeO_2/ASC catalysts have achieved enhanced catalytic activities by doping rare earth metals, especially Nd. In order to investigate the promoting effect of Nd, several characterization techniques including XRD, XPS and Raman have been conducted to study the structural properties of catalysts. Nevertheless, the in situ investigation on the reaction pathway was lacking, which could provide sufficient evidence for the mechanism on the basis of surface adsorption species and the intermediates.

In this paper, the in situ diffuse reflectance infrared Fourier transform spectroscopy (in situ DRIFTS) was used to study the respective adsorbed species of ammonia and nitrogen oxides, as well as their reactive properties during the transient reaction. By means of the DRIFTS spectra and previous structural

analysis, the promotion mechanism of Nd and the reaction pathway of NH_3-SCR over CeO_2/ASC and CeO_2-Nd/ASC were elucidated. The investigations will definitely provide deep insights into the catalyst design for the further enhancement of denitration performance at lower temperature.

2. Experimental

2.1 Catalyst preparation

The catalysts were prepared by hydrothermal method. A proper amount of cerium nitrate was first dissolved in distilled water to prepare the precursor solution (20 wt%). Then 3 g of ASC were added into 25 mL precursor solution, transferred into a stainless steel autoclave and heated at 160 ℃ for 24 h. After the cooling of autoclave to room temperature, the sample was washed with distilled water and dried at 120 ℃ for 5 h, followed by calcination at 700 °C in Ar atmosphere for 4 h with a flow rate of 150 mL/min. The prepared sample was denoted as CeO_2/ASC. When CeO_2/ASC catalyst was doped by Nd, a previously optimized molar ratio of 1:1 was adopted to prepare the precursor solution and the synthesis procedure was the same as that of CeO_2/ASC. The corresponding sample was denoted as CeO_2-Nd/ASC.

2.2 Catalyst characterization

The crystal phases of the samples were analyzed by a powder X-ray diffractometer (XRD, Rigaku Dmax/2400) with Cu Kα radiation at a scanning rate of 8 °/min over the 2θ range of 10-80 °. Surface morphologies of catalysts were characterized by the field emission scanning electron microscope (SEM) operated at 10 kV (Hitachi S-4800). The high-resolution transmission electron microscopy (HRTEM) was carried out on a Tecnai G2 F20 electron microscope with an acceleration voltage of 300 kV. Samples were dispersed in ethanol with ultrasonic treatment and then mounted on a copper-supported carbon polymer grid by placing a few droplets of a suspension on the grid, followed by drying at ambient condition.

2.3 SCR activity measurements

The SCR activity measurement was carried out in a fixed bed quartz reactor (inner diameter 25 mm) in the temperature range of 150-300 °C. 1 gram of catalyst was used in each experiment and the simulated gas

composition was as follows: 1000 ppm NO, 1000 ppm NH_3, 2% O_2 and balance Ar. The total flow rate was 400 mL/min, corresponding to a gas hourly space velocity (GHSV) of 12000 h^{-1}. The concentrations of NO, N_2O, NO_2 and NH_3 at the inlet and outlet were measured by an on-line FTIR spectrophotometer (Nicolet 670). The activity data was collected when the catalytic reaction substantially reached a steady state condition for 1 h at each temperature. NO_x conversion and N_2 selectivity were respectively calculated as follows:

$$NO_x \text{ conversion } (\%) = (1 - \frac{[NO_X]_{out}}{[NO_X]_{in}}) \times 100\%$$

$$N_2 \text{ selectivity } (\%) = (1 - \frac{2[N_2O]_{out}}{[NO_X]_{in} - [NO_X]_{out}}) \times 100\%$$

2.4 In situ DRIFTS studies

The DRIFTS experiments were carried out on a Fourier transform infrared spectrometer (FT-IR, Nicolet 670) equipped with an in situ Harrick DRIFT cell containing ZnSe window and a liquid nitrogen-cooled MCT detector. Prior to the experiments, the catalysts were purged in Ar atmosphere at 300 °C for 1 h to remove the adsorbed impurities. The background spectra of KBr were recorded in Ar and subtracted from the sample spectra. The DRIFTS spectra were collected by accumulating 100 scans with a resolution of 4 cm^{-1}.

3. Results

3.1 Characterization of CeO_2/ASC and CeO_2-Nd/ASC

Fig. 1 showed the XRD patterns and morphologies of CeO_2/ASC and CeO_2-Nd/ASC catalysts. As illustrated in **Fig. 1(a)**, typical CeO_2 patterns were observed for CeO_2/ASC. While for CeO_2-Nd/ASC, no Nd but only CeO_2 were detected with negative frequency shifts comparing to the characteristic peak positions of pure CeO_2. As we have demonstrated,[35] Nd atom with a larger ionic radius, penetrated into the crystal lattice structure of CeO_2 via the formation of solid solutions, resulting in an expansion of lattice and the decrease of peak positions. The SEM images of CeO_2/ASC and CeO_2-Nd/ASC catalysts

were shown in **Fig. 1(b)** and **1(c)**. Both of the catalysts presented a compact rectangular pyramid structure. **Fig. 1(d) and 1(e)** showed the HRTEM images and the corresponding reduced fast Fourier transform (reduced FFT) images of catalysts. It was confirmed from these images that CeO_2/ASC catalyst was single crystalline while CeO_2-Nd/ASC presented a polycrystalline structure, indicating the penetration of Nd into the crystal lattice of CeO_2. The XRD patterns and HRTEM images provided convincing evidence for the generation of solid solution.

3.2 NH_3-SCR activity

The NH_3-SCR performances of CeO_2/ASC and CeO_2-Nd/ASC catalysts in the range of 150-300 °C were shown in **Fig. 2(a)**. It was found that the NO_x conversion of CeO_2/ASC catalyst gradually increased with the elevation of temperature from 40% at 150 °C to about 85% at 250 °C. Compared with CeO_2/ASC, CeO_2-Nd/ASC exhibited a much higher activity and the temperature at 90% conversion decreased to 200 °C. N_2 selectivities of as-prepared samples were illustrated in **Fig. 2(b)**. Few amounts of N_2O were formed over both catalysts, which led to good N_2 selectivities of more than 90%.

3.3 In situ DRIFTS studies

In situ DRIFTS studies were performed to detect the process of denitration reaction through the identification of active sites, adsorbed species and the intermediates on the surface under different conditions, thereby providing evidence for the mechanism analysis. The corresponding band assignments were summarized in **Table 1**.

3.3.1 Adsorption of NH_3

The adsorbed species of NH_3 over CeO_2/ASC and CeO_2-Nd/ASC catalysts were investigated by FT-IR spectroscopy after being exposed to 1000 ppm NH_3/Ar for different time at 200 °C. The adsorption of NH_3 on CeO_2/ASC was illustrated in **Fig. 3(a)**. Distinct bands at 1550, 1513, 965 and 928 cm^{-1} appeared in the initial 3 min. Simultaneously, several weak bands at 1394, 1459 and 1624 cm^{-1} were observed. After 5 min, bands at 1100, 1249 and 3334 cm^{-1} were detected. Notably, the bands at 928 and 965 cm^{-1}

significantly increased. With the further increase of time, the DRIFTS spectra kept relatively stable. With regard to the adsorbed NH_3 coordinated to Lewis acid sites, the bands at 3334 and 1624 cm^{-1} were attributed to the asymmetric stretching vibration and the asymmetric bending vibration of N-H bonds, while bands at 1249 and 1100 cm^{-1} represented the symmetric N-H bending vibration.[38] In terms of the ad-species adsorbed on Brønsted acid sites, the bands at 1459 and in the range of 1640-1850 cm^{-1} represented the asymmetric and symmetric bending vibrations of NH_4^+ species, respectively, and the band at 1394 cm^{-1} corresponded to the deformation modes of NH_4^+.[39] While the bands at 965 and 928 cm^{-1} were assigned to the weakly adsorbed NH_3.[40] Furthermore, the bands observed at 1550 and 1513 cm^{-1} did not belong to the weakly adsorbed species, the Lewis or Brønsted acid sites. Ramis et al.[41] suggested that the band at 1550 cm^{-1} might be attributed to the intermediate from oxidation of NH_3, and Kijlstra et al.[42] proposed that the band at 1510 cm^{-1} might be ascribed to the amide species ($-NH_2$). Accordingly, the bands at 1550 and 1513 cm^{-1} could be assigned to the intermediate from oxidation of NH_3 and amide species, respectively.

Fig. 3(b) showed the DRIFTS spectra of NH_3 adsorption on CeO_2-Nd/ASC, which were much different from the spectra of CeO_2/ASC. As the adsorption proceeded, the bands at 1456 cm^{-1} and in the range of 1640-1850 cm^{-1} were enhanced, which were attributed to NH_4^+ species on Brønsted acid sites. Furthermore, the bands assigned to the intermediate from oxidation of ammonia and amide species (1554 and 1512 cm^{-1}) were also strengthened. However, the coordinated NH_3 on Lewis acid sites at 3334 and 1249 cm^{-1} were hardly detectable. These differences indicated that the addition of Nd could significantly increase both the amount and thermal stability of Brønsted acid sites over CeO_2-Nd/ASC catalyst. Besides, the oxidation from the adsorbed NH_3 species to the intermediates and amide species was also accelerated.

3.3.2 Co-adsorption of NO and O_2

The DRIFTS spectra of NO adsorption were recorded when the catalysts were exposed to 1000 ppm NO + 2% O_2/Ar. The DRIFTS spectra of CeO_2/ASC catalyst at different time were illustrated in **Fig. 4(a)**.

The bands at 1629 and 1593 cm^{-1} due to the adsorbed NO_2 molecules[43] immediately appeared in 3 min. After the adsorption for 5 min, two new bands at 1369 and 1017 cm^{-1} arose, which could be assigned to the nitrate species and cis-$N_2O_2^{2-}$,[43] respectively. The band detected at 1912 cm^{-1} in 10 min was assigned to the gaseous or weakly adsorbed NO.[44] The intensities of all bands gradually increased and then kept stable to 30 min.

Fig. 4(b) showed the DRIFTS spectra of NO adsorbed species on CeO_2-Nd/ASC, which were very similar to the spectra of CeO_2/ASC. In the initial 3 min, the intensities of adsorbed NO_2 (1632 and 1601 cm^{-1}) were extremely strong and a new band due to the nitrate species at 1365 cm^{-1} was observed. With the time increasing, the bands at 1632 and 1601 cm^{-1} became weaker while the band at 1365 cm^{-1} was enhanced, indicating the variation from the adsorbed NO_2 (1632 and 1601 cm^{-1}) into nitrate species (1365 cm^{-1}). The bands at 1910 and 1842 cm^{-1} were assigned to the weakly adsorbed NO. A satellite peak at 965 cm^{-1} near 1006 cm^{-1} appeared which represented the asymmetric stretching vibration of Cis-$N_2O_2^{2-}$. Furthermore, the intensities of characteristic peaks were much stronger than those of CeO_2/ASC, which suggested that the adsorption of NO and further oxidation were considerably promoted upon the Nd modification and thereby favored the "fast SCR" reaction.[35]

3.3.3 Reaction between nitrogen oxides with adsorbed NH_3 species

The catalysts were first exposed to a flow containing 1000 ppm NH_3/Ar at 200 °C for 30 min followed by purging with Ar for 15 min. Afterwards, 1000 ppm NO + 2% O_2/Ar was introduced into the IR cell and the DRIFTS spectra were recorded as a function of time. After the treatment of NH_3 on CeO_2/ASC, coordinated adsorbed NH_3 species on Lewis acid sites (3334, 1624, 1249 and 1100 cm^{-1}), weakly adsorbed NH_3 (965 and 928 cm^{-1}), the intermediates from oxidation of NH_3 (1550 cm^{-1}), amide species (1513 cm^{-1}), and few NH_4^+ species (1394, 1459 and 1640-1850 cm^{-1}) were formed on CeO_2/ASC catalyst as shown in **Fig. 5(a)**. When NO and O_2 was introduced, the intermediate and amide species as well as ammonia ad-species quickly decreased and completely vanished in 5 min. Meanwhile, several new bands

at 1905, 1839, 1631, 1608, 1376, 1010 and 910 cm^{-1}, which were assigned to the adsorbed NO_x species, were detected. As compared to CeO_2/ASC, the bands of NH_4^+ species, the intermediate of oxidation of NH_3 and amide species were much stronger on CeO_2-Nd/ASC (**Fig. 5(b)**) after the adsorption of NH_3. Furthermore, the peaks due to the adsorbed NO_x species in 30 min were more intense. Nevertheless, the bands adsorbed on Lewis acid sites were not detected. Therefore, it suggested that the stable Brønsted acid sites played an important role in the denitration over CeO_2-Nd/ASC.

3.3.4 Reaction between NH_3 and adsorbed nitrogen oxides species

In this experiment, the catalysts were pre-exposed to a flow containing 1000 ppm NO + O_2/Ar at 200 °C for 30 min. After purging with Ar for 15 min, 1000 ppm NH_3 /Ar was introduced into the cell and the DRIFTS spectra were recorded with the variation of time. As shown in **Fig. 6**, the spectra of CeO_2/ASC and CeO_2-Nd/ASC were relatively similar. After the introduction of NH_3, the bands of adsorbed NO_2 species at about 1632 and 1601 cm^{-1} vanished in 3 min. The nitrate species at 1365 cm^{-1} remained stable but shifted to 1380-1390 cm^{-1} due to the reaction with ammonia species.[45] As the reaction proceeded, the weakly adsorbed NH_3 (964 and 929 cm^{-1}), NH_4^+ species on Brønsted acid sites (1392, 1458 and in the range of 1640-1850 cm^{-1}), the intermediates from oxidation of NH_3 (1541 cm^{-1}) and amide species (1510 cm^{-1}) notably increased. The stronger peaks of adsorbed NO_2 species and Cis-$N_2O_2^{2-}$ on CeO_2-Nd/ASC as shown in **Fig. 3(b)**, indicated the enhanced oxidation of NO to NO_2 which might be promoted by rare earth metals.[20] Therefore, rare earth oxides loaded on activated semi-coke, especially rare earth composite oxides might facilitate the proceeding of "fast SCR" process by means of the enhanced oxidation of NO.

3.3.5 DRIFTS spectra in a flow of NO+NH_3+O_2

In order to identify the species present on the catalysts under reaction conditions, the DRIFTS spectra were recorded when the catalysts were heated from 150 °C to 300 °C in a flow of 1000 ppm NO+1000 ppm NH_3+2% O_2. **Fig. 7(a)** showed the spectra of CeO_2/ASC catalyst in a flow of NO+NH_3+O_2. When the

temperature was 150 °C, coordinated NH_3 on Lewis acid sites (3332 and 1258 cm^{-1}), weakly adsorbed NH_3 (965 and 928 cm^{-1}), few NH_4^+ species on Brønsted acid sites (1482, 1438 and in the range of 1640-1850 cm^{-1}), adsorbed NO (1905 and 1842 cm^{-1}) and NO_2 (1630 and 1594 cm^{-1}), nitrate species (1376 cm^{-1}) were observed on the surface. With the increase of temperature, nitrate species and adsorbed NO_2 diminished quickly, while weakly adsorbed NH_3 kept stable. The DRIFTS spectra of CeO_2-Nd/ASC were illustrated in **Fig. 7(b)** Compared with CeO_2/ASC, the intensities of NH_4^+ on Brønsted acid sites (1482, 1438 and in the range of 1640-1850 cm^{-1}), were much stronger on CeO_2-Nd/ASC, which indicated that NH_4^+ on Brønsted acid sites played a vital role in the SCR reaction at low temperature for CeO_2-Nd/ASC.

By careful analysis of the NH_3 adsorbed species, NH species (1436~1460 cm^{-1}) which was originated from the excessive hydrogen abstraction of the coordinated NH_3, was hardly detected over CeO_2/ASC and CeO_2-Nd/ASC catalysts. According to the literatures,[40,46] NH species was unable to react with NO to form N_2 instead of N_2O species. The formation of N_2O was described as follows:

$$NH_{(ads)} \xrightarrow{NO} NHNO_{(ads)} \rightarrow N_2O$$

However in this study, NH species was not found in the DRIFTS spectra, indicating that NH species was difficult to form over CeO_2/ASC and CeO_2-Nd/ASC catalysts. Moreover, in our previous study,[45] the NH species was also not observed on both the ASC and V_2O_5/ASC catalyst. Thus, low amount of N_2O was produced and resulted into good N_2 selectitvities of more than 90%.

4. Discussion

4.1. Denitration mechanism on CeO_2/ASC catalyst

Based on the DRIFTS studies, it could be concluded that ammonia could be adsorbed on Lewis and Brønsted acid sites, giving rise to the appearance of coordinated NH_3, NH_4^+, $-NH_2$ and intermediates from oxidation of NH_3 over CeO_2/ASC (**Fig. 3(a)**). The Lewis acid sites were mainly attributed to Ce^{4+} while Brønsted acid sites were related to Ce^{3+} demonstrated by Wang et al.[35] Furthermore, the quantity of coordinated NH_3 on Lewis acid sites was much higher than that of NH_4^+ species (**Fig. 3(a)**). This was in

accordance with our previous research[35] that Ce^{3+} concentration in CeO_2/ASC was only 9.14%. When $NO+O_2$ was introduced to the surface pretreated with NH_3, all the bands corresponding to the adsorbed NH_3 vanished quickly (**Fig. 5(a)**). Therefore, it was reasonable to deduce that the reaction between NO and coordinated NH_3 on Lewis acid sites dominated.

NO could be adsorbed and further oxidized into NO_2, $N_2O_2^{2-}$ and nitrate species over CeO_2/ASC (**Fig. 4(a)**). It was worth mentioning that the support ASC could facilitate the oxidation of NO and provide the Brønsted acid sites for the adsorption of NH_3, which mainly resulted from the graphite crystalline and the oxygen functional groups as demonstrated in our previous study.[45] When NH_3 was passed over the surface pretreated with NO, the adsorbed NO_2 rapidly decreased，whereas the nitrate species at 1360 cm^{-1} remained stable (**Fig. 6(a)**), indicating that it was NO_2 rather than nitrate species that could react quickly with NH_3. Moreover, the coexistence of nitrate species and adsorbed NH_3 suggested that NH_3 and NO_x were adsorbed at different active sites over the surface of CeO_2/ASC catalyst.

In terms of previous literature studies and the results in this paper, a simplified reaction mechanism on CeO_2/ASC catalysts was proposed and may follow two pathways as illustrated below:

(1) E-R mechanism: the coordinated NH_3 absorbed over Lewis acid sites was first oxidized into amide species, and then reacted directly with gaseous NO into the intermediates which decomposed to produce N_2 and H_2O.

$$NH_3(g) \xrightarrow{Ce^{4+}} NH_3(a) \quad \text{over Lewis acid sites} \qquad (1)$$

$$O_2(g) \rightarrow 2O(a) \qquad (2)$$

$$NH_3(a) + O(a) \rightarrow NH_2(a) + OH(a) \qquad (3)$$

$$NO(g) + NH_2(a) \rightarrow NH_2NO(a) \qquad (4)$$

$$NH_2NO(a) \rightarrow N_2(g) + H_2O \qquad (5)$$

(2) L-H mechanism: (Reaction between the adsorbed NO_2 species and coordinated NH_3)

$$NO + O_2(g) \rightarrow 2NO_2(a) \qquad (6)$$

$$NH_3(g) \xrightarrow{Ce^{4+}} NH_3(a) \quad \text{over Lewis acid sites} \quad (7)$$

$$NO_2(a) + 2\,NH_3(a) \rightarrow NO_2(NH_3)_2 \quad (8)$$

$$NO(g) + NO_2(NH_3)_2 \rightarrow \ldots\ldots \rightarrow 2\,N_2 + 3\,H_2O \quad (9)$$

4.2 Denitration mechanism on CeO_2-Nd/ASC

From our previous study,[35] the addition of Nd brought about the formation of solid solutions with CeO_2 as the solute due to the penetration of Nd atom into the cubic lattice structure of CeO_2. Therefore, the doping of Nd might be conducive to generate more oxygen vacancies and improve the Ce^{3+} concentration, hence playing a vital role in the enhanced catalytic activity over CeO_2-Nd/ASC.

Compared with CeO_2/ASC, the adsorption of NH_3 on CeO_2-Nd/ASC catalyst was very different. The bands assigned to the intermediate from the oxidation of ammonia and amide species (**Fig. 3(b)**) were strengthened. Furthermore, stronger peaks assigned to NH_4^+ (**Fig. 3(b)**) were detected due to the increased quantity of Brønsted acid sites. However, it was reported that NH_4^+ was undetectable on pure CeO_2[43] and extremely weak on ASC[45] during the adsorption of NH_3. More importantly, the undetectable coordinated NH_3 on Lewis acid sites (**Fig. 3(b)**) provided convincing evidence for the transformation of Ce^{4+} to Ce^{3+} upon the addition of Nd. The XPS results[35] revealed the higher Ce^{3+} concentration after the doping of Nd. Thus, the transformation process with the introduction of NH_3 was presented as follows:

$$Ce^{4+}\text{-}NH_3(a) \xrightarrow{Nd^{3+}} Ce^{3+}\text{-}NH_4^+ \quad (10)$$

After NO+O_2 passing over the catalyst, the active ammonia species quickly vanished (**Fig. 5(b)**), indicating the existence of E-R mechanism.

For the adsorption of NO, it was similar to that on CeO_2/ASC except for the greatly increased intensities of adsorbed NO_x species (**Fig. 4(b)**), indicating the enhanced adsorption and oxidation of NO after the Nd modification. From the Raman results,[35] the doping of Nd resulted in more oxygen vacancies and accelerated the migration of oxygen atom between the bulk and surface oxygen atoms, accompanied by the fast and repeatable redox between Ce^{4+} and Ce^{3+} ions. Therefore, the oxidation of NO to NO_2 was

enabled which was coincident with the DRIFTS results in this study. The formation of NO_2 species promoted the proceeding of the "fast SCR" reaction and improved the SCR performance, as the reaction rate of "fast SCR" reaction was at least 10 times higher than that of the well-known "standard SCR" reaction.[47] After the introduction of NH_3, all the adsorbed NO_x species quickly vanished (**Fig. 6(b)**), demonstrating the existence of L-H mechanism.

In view of the DRIFTS results, the SCR reaction of NO with NH_3 over Ce-Nd/ASC catalyst may take place according to two possible pathways and the simplified reactions were presented as follows:

(1) E-R mechanism:

$$NH_3(g) \xrightarrow{Ce^{3+}/Nd^{3+}} NH_4^+(a) \quad \text{over Brønsted acid site} \qquad (11)$$

$$NH_4^+ \rightarrow NH_2(a) + 2H^+ + e^- \qquad (12)$$

$$NO(g) + NH_2(a) \rightarrow NH_2NO(a) \rightarrow N_2 + H_2O \qquad (13)$$

(2) L-H mechanism:

$$NH_3(g) \xrightarrow{Ce^{3+}/Nd^{3+}} NH_4^+(a) \quad \text{over Brønsted acid site} \qquad (14)$$

$$2NO + O_2(g) \rightarrow 2NO_2(a) \qquad (15)$$

$$NH_4^+ + e^- + NO_2 \rightarrow NH_4NO_2 \rightarrow NH_2NO(a) + H_2O \rightarrow N_2 + 2H_2O \qquad (16)$$

$$2H^+ + O(a) \rightarrow H_2O + e^- \qquad (17)$$

4.3 Effect of Nd doping

Combined with the structural analysis[35] and the in situ DRIFTS studies, the promoting effect of Nd was elucidated.

(1) The addition of Nd gave rise to the structural defect of CeO_2 and resulted into the high concentration of Ce^{3+} accompanied by the generation of oxygen vacancy. Consequently, the adsorption of oxygen atom was enhanced due to the charge imbalance and unsaturated chemical bonds on the catalysts surface[35]. Therefore, the oxidation-reduction cycle was accelerated, which was considerably important for the catalytic activity.

(2) Nd modification was favorable for the transformation from Ce^{4+} to Ce^{3+} and thereby more Brønsted acid sites were generated.

(3) The oxygen vacancies facilitated the adsorption and oxidation of NO to NO_2, and thereby favored the denitration.

5 Conclusions

In this study, CeO_2-Nd/ASC catalyst presented much higher denitration performance than CeO_2 /ASC at low temperature. The promotion mechanism of Nd addition was investigated on the basis of in situ DRIFTS studies. It is proposed that the NH_3-SCR process over CeO_2/ASC and CeO_2-Nd/ASC took place according to both E-R and L-H mechanisms. However, the modification of Nd was beneficial for the formation of Ce^{3+} and oxygen vacancies, which promoted the transformation of Lewis acid sites to Brønsted acid sites and the adsorption-oxidation of NO, respectively. In this way, the presence of Ce^{3+} and oxygen vacancies led to the enhanced catalytic activity of CeO_2-Nd/ASC compared with CeO_2 /ASC.

Acknowledgement

Supports by the National High Technology Research and Development Program of China (863 Program, 2012AA06A114), the Key Projects in the National Science & Technology Pillar Program (2013BAC14B07), and Supports by the National Natural Science Foundation of China (51172003，51272005 and 51472006) are acknowledged.

Reference

1 Z. Liang, X. Ma, H. Lin and Y. Tang, *Appl. Energ*, 2011, **88**, 1120.
2 M. Fu, C. Li, P. Lu, L. Qu, M. Zhang, Y. Zhou, M. Yu and Y. Fang, *Catal. Sci. Technol.*, 2014, **4**, 14.
3 L. Zhang, D. Wang, Y. Liu, K. Kamasamudram, J. Li and W. Epling, *Appl. Catal. B*, 2014, **156-157**, 371.
4 Y. Xi, N. A. Ottinger and Z. G. Liu, *Appl. Catal. B*, 2014, **160-161**, 1.
5 F. Tang, B. Xu, H. Shi, J. Qiu and Y. Fan, *Appl. Catal. B*, 2010, **94**, 71.
6 R. Jin, Y. Liu, Z. Wu, H. Wang and T. Gu, *Catal. Today*, 2010, **153**, 84.
7 D. E. Doronkin, T. S. Khan, T. Bligaard, S. Fogel, P. Gabrielsson and S. Dahl, *Appl. Catal. B*, 2012, **117-118**, 49.
8 Z. Zhu, Z. Liu, S. Liu and H. Niu, *Appl. Catal. B*, 1999, **23**, L229.
9 Z. Zhu, H. Niu, Z. Liu, and S. Liu, *J. Catal.*, 2000, **195**, 268.
10 P. Maitarad, J. Han, D. Zhang, L. Shi, S. Namuangruk and T. Rungrotmongkol, *J. Phys. Chemi. C*,

2014, **118**, 9612.
11 C. Li, Q. Li, P. Lu, H. Cui and G. Zeng, *Front. Env. Sci. Eng.*, 2012, **6**, 156.
12 T. Wang, K. Sun, Z. Lu and Y. Zhang, *React. Kinet. Mech. Cat.*, 2010, **101**, 153.
13 B. Shen, T. Liu, N. Zhao, X. Yang and L. Deng, *J. Environ. Sci.*, 2010, **22**, 1447.
14 Y. Shen, Y. Ma and S. Zhu, *Catal. Sci. Technol.*, 2012, **2**, 589.
15 K. Rao and H. Ha, *Catal. Sci. Technol.*, 2012, **2**, 495.
16 F. Liu, W. Shan, Z. Lian, L. Xie, W. Yang and H. He, *Catal. Sci. Technol.*, 2013, **3**, 2699.
17 C. Fang, D. Zhang, L. Shi, R. Gao, H. Li, L. Ye and J. Zhang, *Catal. Sci. Technol.*, 2013, **3**, 803.
18 J. R. H. Carucci, K. Arve, S. Bartova, K. Eranen, T. Salmi and D. Y. Murzin, *Catal. Sci. Technol.*, 2011, **1**, 1456.
19 S. Cai, D. Zhang, L. Zhang, L. Huang, H. Li, R. Gao, L. Shi and J. Zhang, *Catal. Sci. Technol.*, 2014, **4**, 93.
20 L. Chen, Z. Si, X. Wu, D. Weng, R. Ran and J. Yu, *J. Rare Earth.*, 2014, **32**, 907.
21 B. Shen, F. Wang and T. Liu, *Powder Technol.*, 2014, **253**, 152.
22 H. Jiang, J. Zhao, D. Jiang and M. Zhang, *Catal. Lett.*, 2014, **144**, 325.
23 W. Pan, Y. Zhou, R. Guo, W. Zhen, J. Hong, H. Xu, Q. Jin, C. Ding and S. Guo, *Environ. Prog. Sustain.*, 2014, **33**, 385.
24 Z. Liu, S. Zhang, J. Li, J. Zhu and L. Ma, *Appl. Catal. B*, 2014, **158-159**, 11.
25 Z. Liu, S. Zhang, J. Li and L. Ma, *Appl. Catal. B*, 2014, **144**, 90.
26 S. M. Lee, H. H. Lee and S. C. Hong, *Appl. Catal. A*, 2014, **470**, 189.
27 R. Zhang, Q. Zhong, W. Zhao, L. Yu and H. Qu, *Appl. Surf. Sci.*, 2014, **289**, 237.
28 M. C. Shin, J. Kim, J. S. Cha, B. Shin and H. Lee, *J. Korean Inst. Met. Ma.*, 2013, **51**, 57.
29 M. C. Shin, J. S. Cha, B. Shin, H. H. Chun and H. Lee, *Electron. Mater. Lett.*, 2013, **9**, 71.
30 L. Chen, J. Li and M. Ge, *Environ. Sci. Technol.*, 2010, **44**, 9590.
31 X. Wang, Y. Zheng, Z. Xu, Y. Liu and X. L. Wang, *Catal. Sci. Technol.*, 2014, **4**, 1738.
32 W. Shan, F. Liu, H. He, X. Shi and Changbin Zhang, *Catal. Today*, 2012, **184**, 160.
33 Z. Zeng, P. Lu, C. Li, G. M. Zeng, X. Jiang, Y. Zhai and X. Fan, *Environ. Technol.*, 2012, **33**, 1331.
34 Z. Lian, F. Liu and Hong He, *Catal. Sci. Technol.*, 2015, **5**, 389.
35 J. Wang, Z. Yan, L. Liu, Y. Zhang, Z. Zhang and X. Wang, *Appl. Surf. Sci.*, 2014, **309**, 1.
36 W. Shan, F. Liu, H. He, X. Shi and C. Zhang, *Chem. Comm.*, 2011, **47**, 8046.
37 F. Liu, Y. Yu and H. He, *Chem. Comm.*, 2014, **50**, 8445.
38 R. Jin, Y. Liu, Y. Wang, W. Cen, Z. Wu, H. Wang and X. Weng, *Appl. Catal. B*, 2014, **148-149**, 582.
39 S. Lin, A. C. Gluhoi and B. E. Nieuwenhuys, *Catal. Today*, 2004, **90**, 3.
40 Y. Liu, T. Gu, X. Weng, Y. Wang, Z. Wu and H. Wang, *J. Phys. Chem. C*, 2012, **116**, 16582.
41 G. Ramis, G. Busca and F. Bregani, *Appl. Catal.*, 1990, **64**, 259.
42 W. S. Kijlstra, D. S. Brands, E. K. Poels and A. Bliek, *J. Catal.*, 1997, **171**, 208.
43 G. Qi, R. T. Yang and R. Chang, *Appl. Catal. B*, 2004, **51**, 93.
44 K. I. Hadjiivanov, *Catal. Rev.*, 2000, **42**, 71.
45 Wang, Z. Yan, L. Liu, Y. Chen, Z. Zhang and X. Wang, *Appl. Surf. Sci.*, 2014, **313**, 660.
46 F. Kapteijn, L. Singoredjo, A. Andreini and J. A. Moulijn, *Appl. Catal. B.*, 1994, **3**, 173.
47 M. Koebel, M. Elsener and G. Madia, Ind. Eng. *Chem. Res.*, 2001, **40**, 52.

Table and Figure Capture

Table 1 Assignment for FTIR bands.

Fig. 1 XRD patterns of CeO_2/ASC and CeO_2-Nd/ASC (a); SEM images of CeO_2/ASC (b) and CeO_2-Nd/ASC (c); HRTEM images of CeO_2/ASC (d) and CeO_2-Nd/ASC (e). The insets in (d) and (e) are the reduced FFT images.

Fig. 2 NH_3-SCR performances of CeO_2/ASC and CeO_2-Nd/ASC catalysts with the variation of temperature: (a) NO conversion, (b) N_2 selectivity.

Fig. 3 DRIFTS spectra of CeO_2/ASC (a) and CeO_2-Nd/ASC (b) exposed to 1000 ppm NH_3 at 200 °C for different time.

Fig. 4 DRIFTS spectra of CeO_2/ASC (a) and CeO_2-Nd/ASC (b) exposed to 1000 ppm NO+2% O_2 at 200 °C for different time.

Fig. 5 DRIFTS spectra of CeO_2/ASC (a) and CeO_2-Nd/ASC (b) pretreated with 1000 ppm NH_3 followed by exposure to 1000 ppm NO +2% O_2 at 200 °C for different time.

Fig. 6 DRIFTS spectra of CeO_2/ASC (a) and CeO_2-Nd/ASC (b) pretreated with 1000 ppm NO +2% O_2 followed by exposure to 1000 ppm NH_3 at 200 °C for different time.

Fig.7 DRIFTS spectra of CeO_2/ASC (a) and CeO_2-Nd/ASC (b) in a flow of 1000 ppm NO + 1000 ppm NH_3 + 2% O_2 at 150, 200, 250 and 300 ^oC.

Table 1 Assignment for FTIR bands.

Bands (cm^{-1})	Assignment	Reference
928, 965	weakly adsorbed NH_3	[40]
1394	deformation modes of NH_4^+	[39]
1459	asymmetric bending vibrations of NH_4^+ species on Brønsted acid sites	[39]
1640-1850	symmetric bending vibrations of NH_4^+ species on Brønsted acid sites	[39]
1624	asymmetric bending vibration of the N-H bonds in coordinated NH_3 on Lewis acid sites	[38]
1100, 1249	symmetric bending vibration of the N-H bonds in coordinated NH_3 on Lewis acid sites	[38]
3334	asymmetric stretching vibration of the N-H bonds in coordinated NH_3 on Lewis acid sites	[38]
1550	the intermediate from oxidation of NH_3	[41]
1513	amide species	[42]
1629, 1593	the adsorbed NO_2 molecules	[43]
1369	nitrate species	[43]
1017	cis-$N_2O_2^{2-}$	[43]
1912, 1842	gaseous or weakly adsorbed NO	[44]

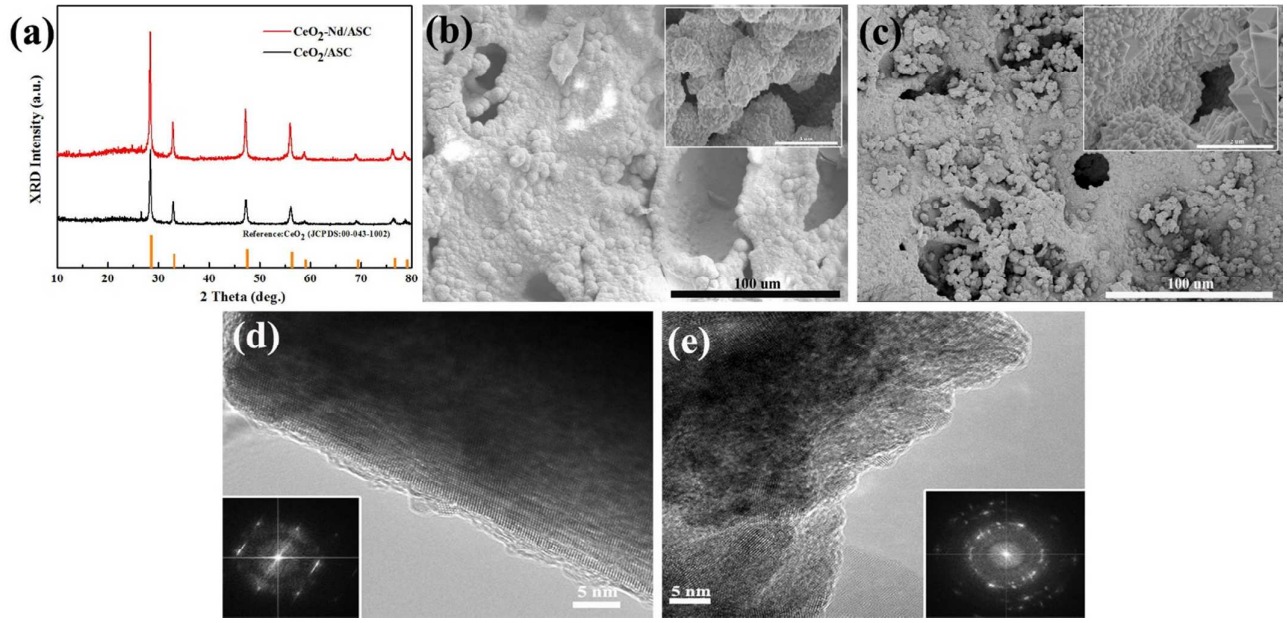

Fig. 1 XRD patterns of CeO_2/ASC and CeO_2-Nd/ASC (a); SEM images of CeO_2/ASC (b) and CeO_2-Nd/ASC (c); HRTEM images of CeO_2/ASC (d) and CeO_2-Nd/ASC (e). The insets in (d) and (e) are the reduced FFT images.

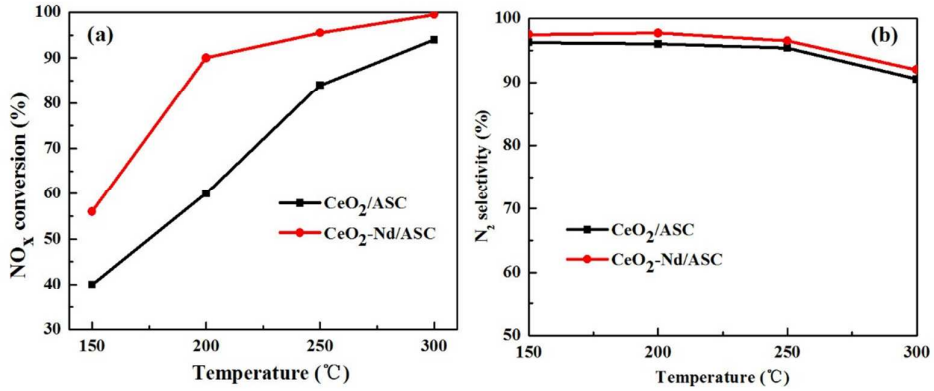

Fig. 2 NH_3-SCR performances of CeO_2/ASC and CeO_2-Nd/ASC catalysts with the variation of temperature: (a) NO conversion, (b) N_2 selectivity. Reaction conditions: 1000 ppm NO, 1000 ppm NH_3, 2% O_2, Ar as the balance gas, GHSV: 12000 h^{-1}.

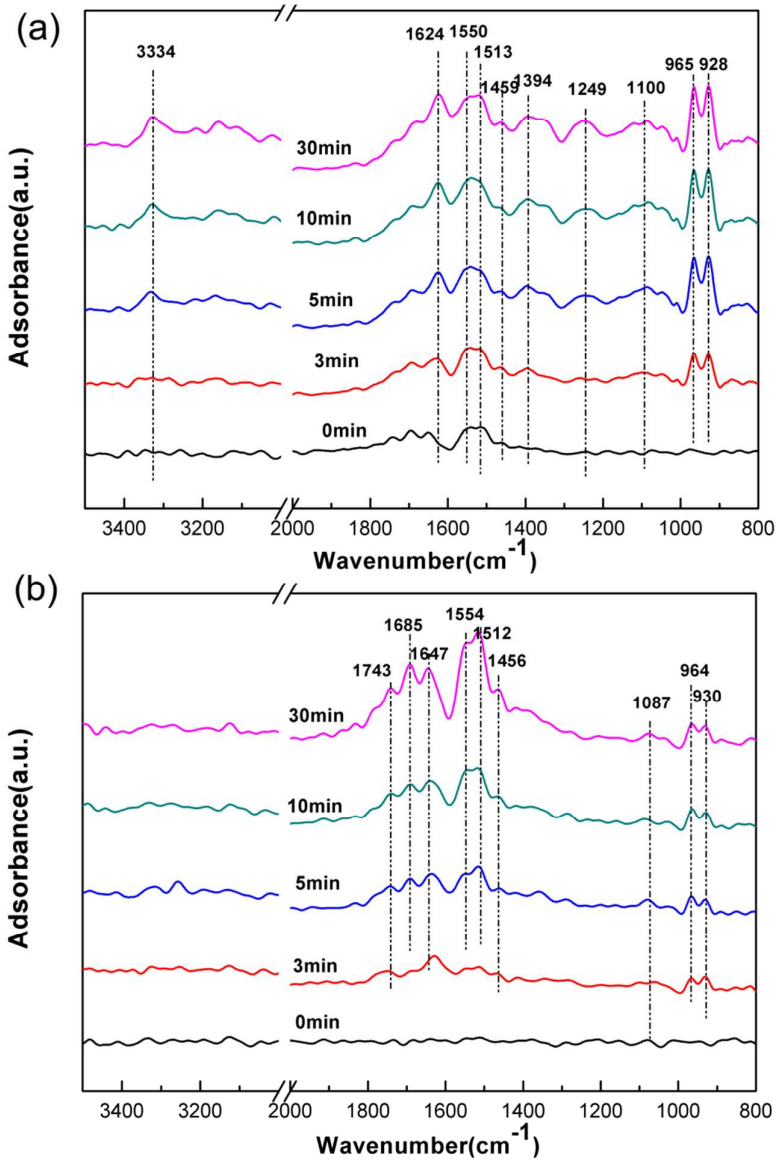

Fig. 3 DRIFTS spectra of CeO_2/ASC (a) and CeO_2-Nd/ASC (b) exposed to 1000 ppm NH_3 at 200 °C for different time.

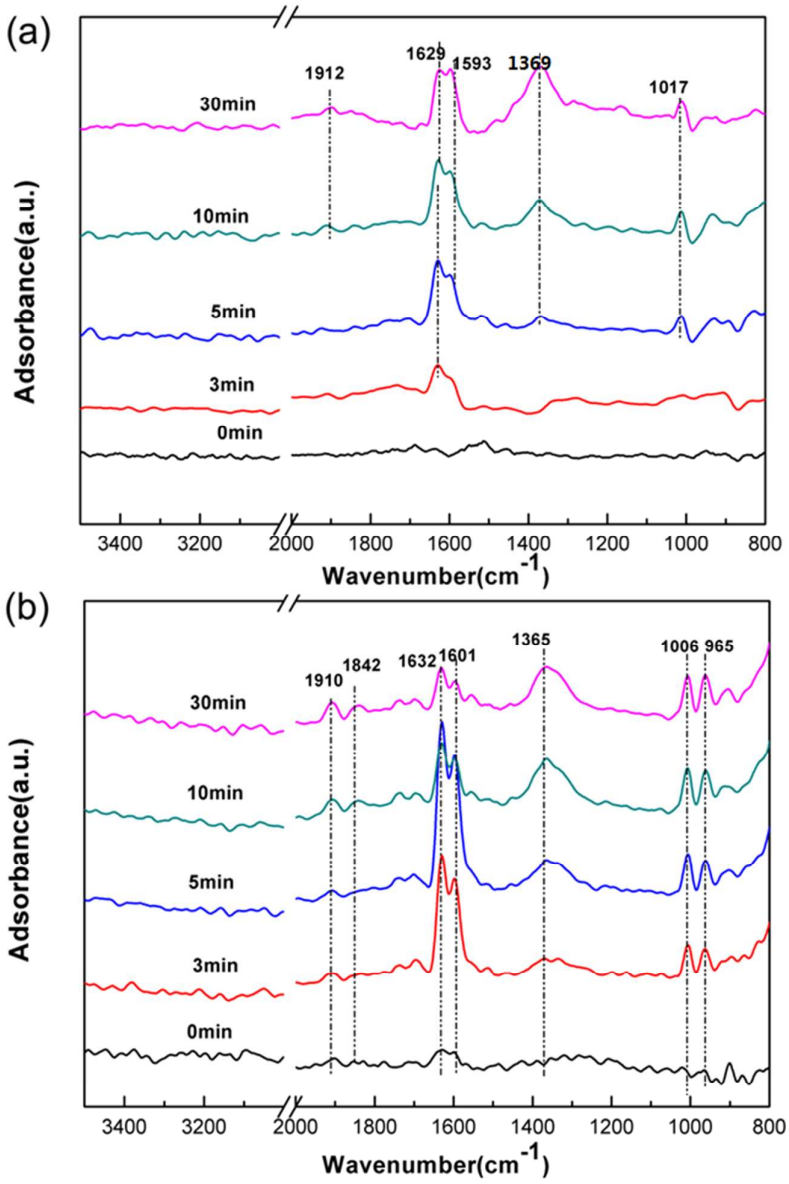

Fig. 4 DRIFTS spectra of CeO_2/ASC (a) and CeO_2-Nd/ASC (b) exposed to 1000 ppm NO+2% O_2 at 200 °C for different time.

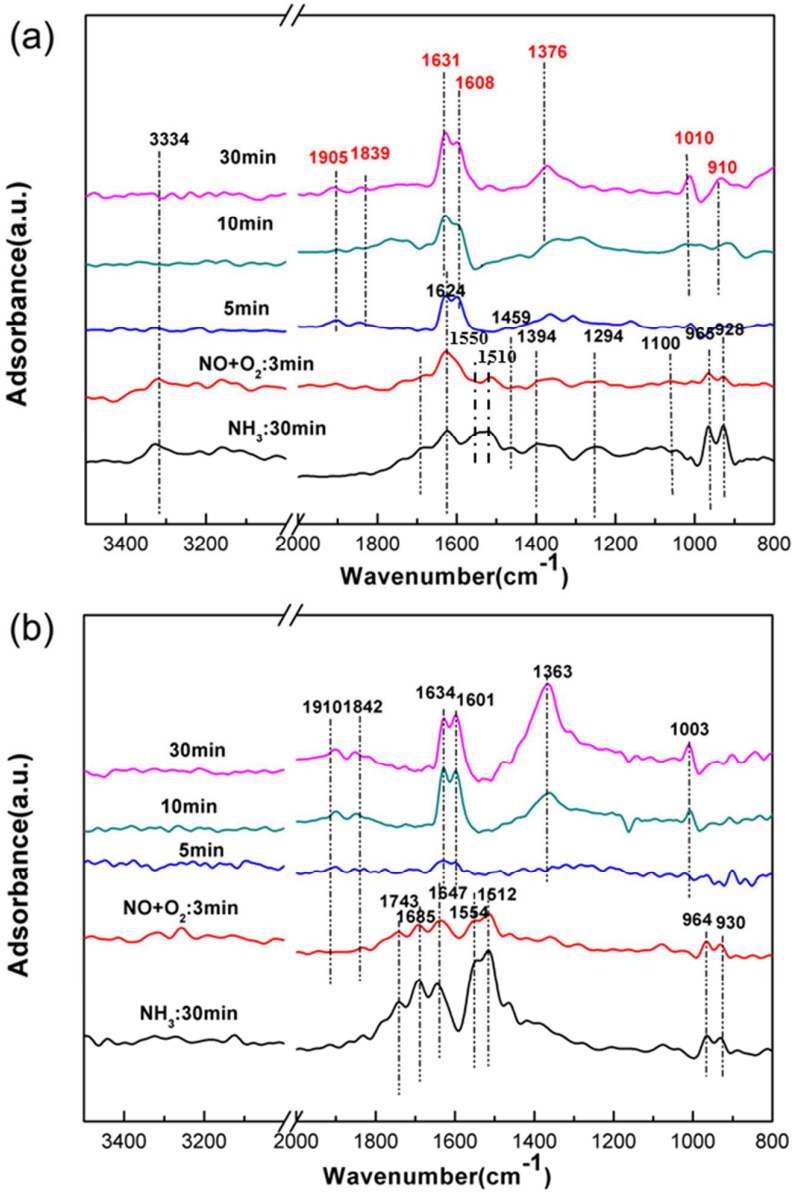

Fig. 5 DRIFTS spectra of CeO_2/ASC (a) and CeO_2-Nd/ASC (b) pretreated with 1000 ppm NH_3 followed by exposure to 1000 ppm NO +2% O_2 at 200 °C for different time.

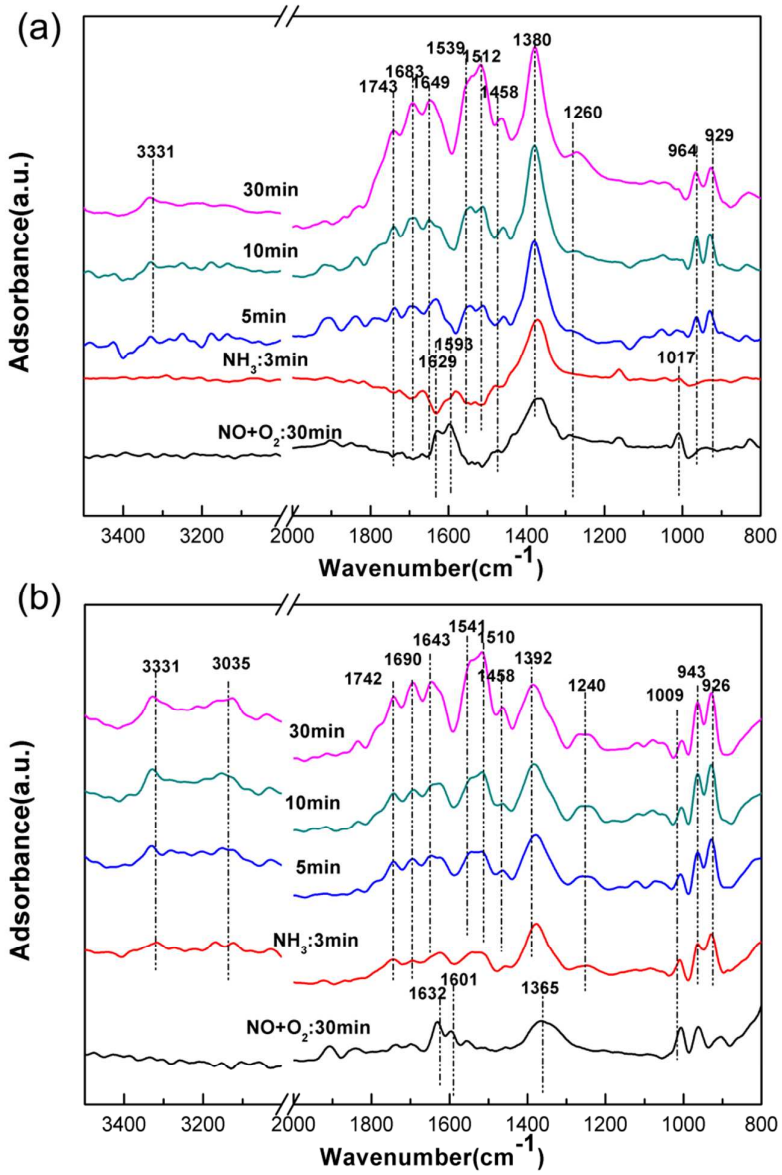

Fig. 6 DRIFTS spectra of CeO_2/ASC (a) and CeO_2-Nd/ASC (b) pretreated with 1000 ppm NO +2% O_2 followed by exposure to 1000 ppm NH_3 at 200 ℃ for different time.

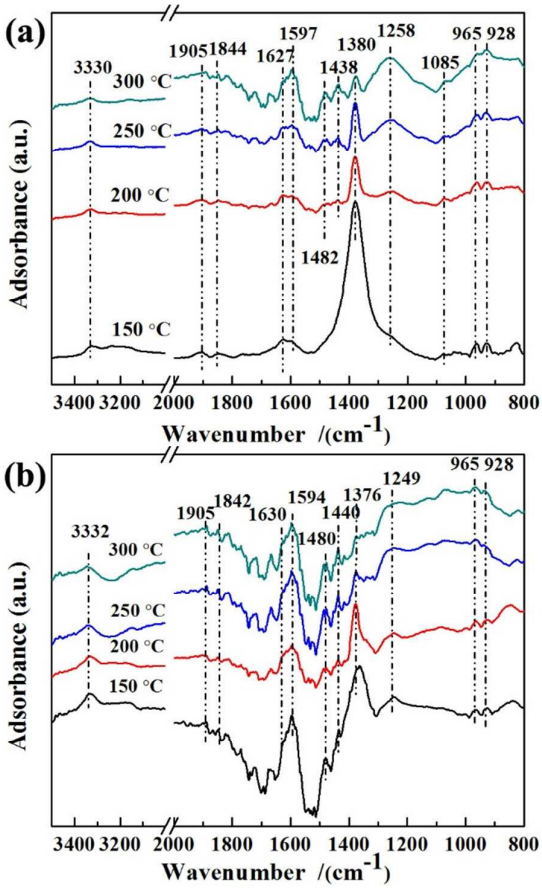

Fig. 7 DRIFTS spectra of CeO_2/ASC (a) and CeO_2-Nd/ASC (b) in a flow of 1000 ppm NO + 1000 ppm NH_3 + 2% O_2 at 150, 200, 250 and 300 ^oC.